LA-UR- 09-00602

Approved for public release;
distribution is unlimited.

Title:	Ideal Magnetophydrodynamic Simulations for Low Beta Compact Toroid Injection into a Hot Strongly Magnetized Plasma
Author(s):	Wei Liu Scott Hsu Hui Li
Intended for:	Physics of Plasma Journal

Los Alamos
NATIONAL LABORATORY
EST. 1943

Form 836 (7/06)

Ideal Magnetohydrodynamic Simulations of Low Beta Compact Toroid Injection into a Hot Strongly Magnetized Plasma

Wei Liu,[1] Scott C. Hsu,[2] and Hui Li[1]

[1] *Theoretical Division, Los Alamos National Lab, Los Alamos, NM, USA, 87545*

[2] *Physics Division, Los Alamos National Lab, Los Alamos, NM, USA, 87545*

Abstract

We present results from three-dimensional ideal magnetohydrodynamic simulations of low β compact toroid (CT) injection into a hot strongly magnetized plasma, with the aim of providing insight into CT fueling of a tokamak with parameters relevant for ITER (International Thermonuclear Experimental Reactor). A regime is identified in terms of CT injection speed and CT-to-background magnetic field ratio that appears promising for precise core fueling. Shock-dominated regimes, which are probably unfavorable for tokamak fueling, are also identified. The CT penetration depth is proportional to the CT injection speed and density. The entire CT evolution can be divided into three stages: (1) initial penetration, (2) compression in the direction of propagation and reconnection, and (3) coming to rest and spreading in the direction perpendicular to injection. Tilting of the CT is not observed due to the fast transit time of the CT across the background plasma.

I. INTRODUCTION

It is important to deliver fuel into the core of a tokamak fusion plasma to maintain steady-state operation, achieve more efficient utilization of deuterium-tritium fuel, and optimize the energy confinement time.[1] Several fueling schemes have been proposed, such as edge gas puffing,[2] pellet injection,[3] and compact toroid (CT) injection.[4] Among them, CT fueling is considered to be the most promising method for core fueling because the injection speed via this method is far higher than those of the other methods. Although extensive worldwide efforts have been devoted to study CT fueling theoretically,[1,4,5] numerically,[6–9] and experimentally,[10–26] the dynamics of core CT fueling of large devices like ITER (International Thermonuclear Experimental Reactor)[27] is not well understood. CT injection has the potential to deposit fuel in a *controlled* manner at any point in the machine, from the edge to the core. Tangential (toroidal) injection can impart momentum for improving plasma β and stability.[28] In a burning plasma device with only radio-frequency (rf) for auxiliary current drive, a CT injection system may be the only internal profile control tool for optimizing bootstrap current and maintaining optimized fusion burn conditions. CT fueling also provides a good chance to study core transport in present machines, helium ash removal studies, and Edge Localized Mode (ELM)[29] control.

In this work, we employ a simple idealized model of a low β CT propagating into a uniform slab plasma with a uniform magnetic field perpendicular to the CT injection direction. This model helps us identify different regimes of operation in terms of CT injection speed, density, and magnetic field strength, as well as understand the essential physics occurring during CT injection. More realistic scenarios, including the use of realistic tokamak profiles and geometry in the background plasma as well as high β CT's, are planned for follow-on research. Compared to past work on CT injection simulations, we have investigated new regimes especially in terms of higher injection velocity and a more ITER-relevant ratio (at least for low β CT's such as spheromaks) of CT-to-background magnetic field (~ 0.1). Simulations with higher injection velocity were made possible by the shock-handling capability of our three-dimensional (3D) ideal magnetohydrodynamic (MHD) code,[30] which was originally developed for plasma astrophysics problems. The lower CT-to-background magnetic field ratios, compared to past work, was enabled by the higher resolution of our code which allowed the boundary layer between the CT and background plasma to be properly resolved.

The paper is organized as follows. In Sec. II, we describe the problem setup including initialization of the CT and background slab plasma. We present the simulation results in Sec. III, and our conclusions and implications for future CT fueling experiments are in Sec. IV.

II. PROBLEM SETUP

A low β CT with spherical radius $r_b = 1$, centered initially at $x_b = 0$, $y_b = 0$ and $z_b = z_{b,0} = -12$, is injected along the z axis into a lower density background plasma with injection velocity $v_{\rm inj}$ (see Fig. 1). The basic model assumptions and numerical treatments are briefly summarized here; they are essentially the same as those in Li et al.[31] where more details are given. The nonlinear system of time-dependent ideal MHD equations in 3D Cartesian coordinates (x, y, z) is given here:

$$\frac{\partial \rho}{\partial t} + \nabla \cdot (\rho \vec{v}) = 0, \tag{1}$$

$$\frac{\partial (\rho \vec{v})}{\partial t} + \nabla \cdot \left(\rho \vec{v}\vec{v} + (p + \frac{B^2}{2})\mathbf{I} - \vec{B}\vec{B} \right) = 0, \tag{2}$$

$$\frac{\partial E}{\partial t} + \nabla \cdot \left[\left(E + p + \frac{B^2}{2} \right) \vec{v} - \vec{B}(\vec{v} \cdot \vec{B}) \right] = 0, \tag{3}$$

$$\frac{\partial \vec{B}}{\partial t} - \nabla \times (\vec{v} \times \vec{B}) = 0, \tag{4}$$

in which ρ, p, $\vec{v}$, $\vec{B}$ and E are the density, (gas) pressure, flow velocity, magnetic field, and total energy, respectively. $\mathbf{I}$ is the unit diagonal tensor. The total energy is $E = p/(\gamma - 1) + \rho v^2/2 + B^2/2$, where γ is the ratio of the specific heats. Note that a factor of $\sqrt{4\pi}$ has been absorbed into the scaling for both the magnetic field $\vec{B}$ and current density $\vec{j}$. All simulations were performed on the parallel Linux clusters at Los Alamos National Laboratory. It should be noted that the details of effects such as reconnection and heat evolution could not be addressed accurately due to the ideal MHD model and the use of a simplified energy equation.

It is well established empirically in coaxial gun spheromak experiments that, under proper conditions, a spheromak "magnetic bubble" (a low β CT) will be formed by the gun discharge.[32] In our simulations, we do not model the CT formation process and instead start with a pre-formed CT moving toward the background slab plasma at speed $v_{\rm inj}$. The stationary background plasma is composed of a slab plasma confined by a uniform background

magnetic field B_p in the x direction. For simplicity, we assume the background plasma has uniform initial number density $\rho_p = 0.1$ and uniform initial temperature $T_p = 0.1$.

In the simulations reported here, the CT structure is similar to the one given in Liu et al.[33] The density profile of the CT plasma with radius $r_b = 1$ is given by

$$\rho_b \propto r_c^2 \exp[-r_c^2 - (z_c - z_b)^2],$$

up to a normalization coefficient and a uniform temperature T_b, where $r_c = \sqrt{x^2 + y^2}$ and $z_c = z$ (see Fig. 1). The density profile used here has its peak shifted from the center of the CT, approximating a spheromak.

The CT magnetic field is determined by three key quantities: the length scale of the bubble magnetic field $r_B = 2$, the amount of poloidal flux Ψ_p, and the index α, which is the ratio of the CT toroidal to poloidal magnetic fields. For simplicity, the CT magnetic field $\vec{B}_\mathrm{b}$ is also assumed to be axisymmetric. The poloidal flux function Ψ_p is specified as

$$\Psi_p \propto r_c^2 \exp[-r_c^2 - (z_c - z_b)^2]\,. \tag{5}$$

The poloidal fields, up to a normalization coefficient, are

$$B_{\mathrm{b},r_c} = -\frac{1}{r_c}\frac{\partial \Psi_p}{\partial z_c}, \quad B_{\mathrm{b},z_c} = \frac{1}{r_c}\frac{\partial \Psi_p}{\partial r_c}, \tag{6}$$

while the toroidal magnetic field is

$$B_{\mathrm{b},\varphi_c} = \frac{\alpha \Psi_p}{r_c} = \alpha r_c \exp[-r_c^2 - (z_c - z_b)^2]\,. \tag{7}$$

The azimuthal component of the CT Lorentz force is zero, but the total azimuthal Lorentz force due to the *combined* fields and currents of the CT may be non-zero.

The CT also has uniform injection velocity v_inj and uniform rotation angular speed ω. In this paper the ratio of the CT's toroidal to poloidal magnetic fields α, the rotation speed of the CT ω, and the specific heat γ are taken to be $\sqrt{10}$, 0 and 5/3, respectively. Physical quantities are normalized by the characteristic system length scale $R_0 = 10$ cm, density $\rho_0 = 7.77 \times 10^{-9}$ g/cm^{-3} (corresponding to plasma number density, which is the sum of electron and ion number density, of 18.6×10^{14} cm^{-3}), and velocity $V_0 = 1.7 \times 10^8$ cm s^{-1}. Other quantities are normalized as: time $t = 1$ gives $R_0/V_0 = 5.9 \times 10^{-8}$ s, magnetic field $B = 1$ gives $(4\pi\rho_0 V_0^2)^{1/2} = 5.3 \times 10^4$ G, and energy $E = 1$ gives $\rho_0 V_0^2 R_0^3 = 2.24 \times 10^{11}$ ergs.

The boundary conditions are all perfectly conducting in the y and z directions except at the port where the CT is injected, while in the x direction outflow boundary conditions are employed in order to mimic the toroidal geometry of a tokamak. Suzuki et al. has pointed out that the boundary condition in the background magnetic field (x) direction is important, *i.e.*, magnetic reconnection has more influence on CT deceleration with perfectly conducting boundary conditions than with stress-free boundary conditions such as outflow and periodic boundary conditions.[8] The total computational domain is $|x| \leq 9$, $|y| \leq 9$, and $|z| \leq 9$, corresponding to a $(180\ \mathrm{cm})^3$ box in actual length units (assuming the physical dimension of the injected CT radius $r_b = 10$ cm). The numerical resolution used here is $400 \times 400 \times 800$, where the grid points are assigned uniformly in the x, y, and z directions. A cell δx $(= \delta y = 2\delta z = 0.045)$ corresponds to 0.45 cm.

III. RESULTS

In this section we present ideal MHD simulation results on the injection of a low β CT into a hot strongly magnetized plasma. We organize our results into three topics: (1) parameter regimes, in terms of v_{inj} and ratio of CT-to-background magnetic field, of CT evolution including the identification of a promising regime for ITER-relevant precise core fueling, (2) detailed description of the CT evolution for the ITER-relevant regime, and (3) dependence of the CT penetration depth on v_{inj} and the initial CT density.

A. Parameter regimes of CT injection

Based on our simulation results, we find that the evolution of the injected CT depends predominantly on the initial injection speed v_{inj} and the initial ratio of CT-to-background magnetic field. As shown in Figure 2, there are several qualitatively distinct regimes of CT injection in terms of the above two parameters.

First, below a threshold injection speed V_{AC}, the CT is unable to penetrate the background plasma at all. This threshold is determined by the requirement that the initial CT kinematic energy exceeds the background magnetic field energy excluded by the CT volume,

$$\frac{1}{2}\rho_b v_{\mathrm{inj}}^2 > \frac{1}{2}B_p^2 \rightarrow v_{\mathrm{inj}} > V_{\mathrm{AC}} = \frac{B_p}{\sqrt{\rho_b}}. \tag{8}$$

This result is consistent with the results of the conducting sphere (CS) model.[1]

Second, above a different threshold injection speed $V_{\rm AP}$, a strong shock and wavefront are observed to develop ahead of the CT, dominating the system evolution (see *left* panel of Fig. 3). This threshold is determined by the condition when $v_{\rm inj}$ exceeds the Alfvén speed of the background plasma, *i.e.*, $v_{\rm inj} > V_{\rm AP} = B_p/\sqrt{\rho_p}$. This shock/wavefront-dominated regime is probably not favorable for CT fueling because it may strongly perturb the tokamak equilibrium. Also, in this case the CT deposition is highly nonlocal (*left* panel of Fig. 3). For comparison, the result ($v_{\rm inj} = 1.1$) without shock/wavefront development is also presented (*right* panel of Fig. 3).

Third, in the regime $V_{\rm AC} < v_{\rm inj} \lesssim V_{\rm AP}$, CT evolution is further determined by the ratio $S_r = B_b/B_p$ of the CT field B_b to the background plasma magnetic field B_p. If $S_r \gg 10$, a large non-zero initial Lorentz force results in strong CT expansion that also leads to the development of a shock and a wavefront that dominate the system evolution.[33] As stated above, this does not favor controlled plasma fueling. In the regime $1 < S_r \lesssim 10$, which is the regime Suzuki et al. have discussed extensively[6–8], the CT is decelerated by both the magnetic pressure and magnetic tension forces. In this regime, the CT tilts while reconnection occurs between the CT and background plasma magnetic fields. Suzuki et al. proposed the Non-slipping Conducting Sphere (NS) model,[6–8] which matches their simulation results pretty well. Our simulation results in this regime verify their conclusions. Because it is difficult for the CT field B_b generated by a co-axial gun to be larger than the tokamak field B_p of several Tesla or more, it is important to explore the regime $S_r < 1$, which is the primary focus of the remainder of this paper. We have identified this regime (*right* panel of Fig. 3) as a promising one for CT fueling of ITER-relevant plasmas due to the precise spatial deposition of the CT and the deep penetration that can be achieved for core fueling applications.

B. Evolution

In this sub-section, we describe in detail the CT evolution for the ITER-relevant regime of $V_{\rm AC} < v_{\rm inj} \lesssim V_{\rm AP}$ and $S_r < 1$. In this regime, the CT evolution can be divided into three stages: (1) initial CT penetration, (2) CT compression in the propagation direction (z) and reconnection, and (3) coming to rest and spreading in the x (toroidal) direction. Magnetic reconnection, starting late in the second stage in our simulations, arises due to numerical

diffusion and leads to mixing between the CT and background plasmas.

In order to mimic CT injection with ITER-relevance, we adopt physical quantities as given in Table I and choose the injection speed $v_{\rm inj}$ such that $V_{\rm AC} = 1.0 < v_{\rm inj} = 1.1 < V_{\rm AP} = 3.16$ (this falls into the "ITER-relevant" case of Fig. 2). Figure 4 displays the time evolution of the plasma density (color contours in common logarithmic scale) in the x-z plane with $y = 0$. The white solid contour lines indicate the magnetic pressure $p_B = B^2/2$. The entire evolution can be described by the three stages mentioned above.

Figure 5 displays the magnetic field B_{xz}, (arrows) and current density j_y (color contours) in the x-z plane at $y = 0$. During the first stage (initial penetration), the CT experiences a very strong magnetic obstacle, and therefore the CT plasma is highly compressed and the plasma density increases at the interface between the CT and background plasmas. A large plasma current also appears at the interface due to the compression of the background magnetic field seen in Fig. 5(a). This current sheet is bent and broken into two parts (Fig. 5(b)) due to the magnetic field configuration of the CT field. Some reconnection takes place at the left part of the current sheet as shown in Fig. 6. The CT is successively decelerated by the magnetic tension force of the background magnetic field.

After the CT has fully entered the background plasma region (after $t \sim 4$), the background field lines, some of which have reconnected with the CT magnetic field at the CT's leading edge, are reconnected again with the CT magnetic field at the CT's trailing edge, as seen in Fig. 5(c). As pointed out by Suzuki et al.[6], via this process the CT is separated from the background fields lines, through which the magnetic tension force decelerating the CT is relaxed. At $t = 4.375$, a magnetic configuration schematically shown in Fig. 6 is formed. This interpretation is supported by Fig. 7, which displays the axial distributions of density and B_x. From Fig. 7, we can see that B_x changes sign from positive to negative and then to positive again. The transition from positive to negative happens at larger z (after the density peak) on the left hand side while at smaller z on the right hand side (before the density peak), which is the case in Fig. 6(*right*) (see two dashed lines in Fig. 6(*right*)). From Fig. 6, primary reconnection sites are at the upper left and lower right sections of the CT. The reconnection process allows the high-density CT plasma to escape from the CT and eventually flow outward along the background magnetic field horizontally (Fig. 6). The CT plasma starts to contract in z and expand in x. The reconnection is asymmetric about the CT axis, and this asymmetry results in CT plasma outflow in a direction that is not

completely in the x direction, but rather obliquely (panel (d) of Fig. 5). Eventually it will become more parallel to x. Magnetic flux is being destroyed as well. During this process the MHD wave drag from Alfvén waves induced by horizontal plasma outflow[1,5] might further slow down the CT plasma. Note that Suzuki et al.[8] showed that the CT penetration depth, based on a model with magnetic tension force as the main deceleration mechanism, matches simulation results very well, implying that MHD wave drag forces may not be important in CT deceleration. The initially injected magnetic and perpendicular kinematic energies are converted into parallel kinematic energy. Contrary to Parks[1] and Suzuki et al.[6,7,8] CT tilting, the time scale of which is proportional to $\sqrt{B_b B_p/\rho_b}$, is not observed in our case due to the fast injection and short CT transit time as required for the ITER-relevant regime (Table I).

After the high-density CT plasma has been depleted during the compression stage (after $t \sim 9$), the CT field diminishes and only the slightly perturbed background field survives, almost orienting to the direction of the initial background magnetic field (see Fig. 4 and Fig. 5(d)). Almost all of the initially injected magnetic and kinematic energy now survive in the form of parallel kinematic energy. The CT comes to rest in the injection direction (z). A narrow elongated structure along x results, as seen in the lower middle and lower right panels of Fig. 4. This line-shaped structure with a spread of only $\Delta z \sim 0.2$ (much smaller than the size of the background plasma) implies a very precise fuel deposition capability.

C. CT penetration depth

In this sub-section, we establish the dependence of CT penetration depth, an important parameter for CT fueling of tokamaks, on the experimentally controllable parameters of CT injection speed $v_{\rm inj}$ and initial density ρ_b, which collectively determine the initial CT energy. The penetration depth S is defined as the axial (z) distance between the final mean position of the injected CT and the injection location on the boundary. We find that S is highly dependent on the initial injection speed $v_{\rm inj}$ and CT density ρ_b. Fig. 8(a) displays the relationship between the S and $v_{\rm inj}$, showing that S is proportional to $v_{\rm inj}$ if $V_{\rm AC} < v_{\rm inj} < V_{\rm AP}$. Fig. 8(b) displays the relationship between the CT density and penetration depth, which shows that the penetration depth S increases with the CT density. The CT spread in the z direction is around ~ 0.2 in all cases, which is very tiny compared to the background plasma

size ~ 20. These two empirical relationships are important in the sense that they provide clues for how to choose the injection speed and CT density to get precise fuel deposition, therefore controlling the core plasma profile in a large tokamak such as *ITER*. It is very hard to manage that by other methods such as pellet injection.[26]

For the case shown in Fig. 8(b), the parameters given in Table I are adopted ($v_{\rm inj} = 2.0$) except CT density ρ_b and CT field B_b. We choose them such that the plasma parameter $\beta = 0.2$ is kept constant for all the simulation results shown in Fig. 8(b). We keep β constant since experimentally this is more reasonable than changing CT density or CT field strength independently. Thus, increasing CT density means increasing both the initial kinematic energy $E_k = \int 1/2 \rho_b v_{\rm inj}^2 dV$, where dV is the infinitesimal CT volume, and initial magnetic energy $E_m = \int 1/2 B_b^2 dV$. However, because of the limiting criterion Eq. 8, the initial CT kinematic energy E_k should be much larger than the initial CT magnetic energy E_m since the background field is much larger than the CT field in all simulation results presented in Fig. 8(b). Also the residual initial total force $\mathbf{j} \times \mathbf{B} - \nabla p$ is proportional to the CT density $\sim O(\rho_b)$. Therefore, increasing the CT density ρ_b would elevate the initial residual force, which would result in shock/wavefronts. Thus, with too large a density ratio ($\rho_b/\rho_p \gtrsim 15$), the fueling is not as localized as the case with smaller CT density, while generating similar phenomena as the shock/wavefront dominated cases.

Results of Fig. 8 remind us of the importance of initially injected energy upon the penetration depth. As discussed in §III B, how long the compression stage lasts is determined by the sum of the initially injected kinematic and magnetic energy. The larger the sum is, the longer it will take for the reconnection to dissipate/convert the energy. If we assume that the deceleration mechanism of the CT is mainly due to the magnetic tension force, which is independent of the initially injected energy,[8] then the larger initially injected energy would lead to deeper fueling given the same injection speed $v_{\rm inj}$ (since plasma parameter $\beta \ll 1$, the internal energy of the CT plasma can be ignored). Certainly the larger injection speed would lead to deeper penetration.

Fig. 9 shows the time evolution of the net toroidal magnetic flux $\psi_t = \int B_y dS$ (only positive B_y is selected) with $v_{\rm inj} = 1.1$ and $\rho_b/\rho_p = 10$. Before $t = 6.25$, the net toroidal magnetic flux increases due to the initial penetration and compression of the magnetic field lines at the interface of the CT and background plasma. After $t = 11.25$, the line structure reaches the horizontal boundaries and some toroidal magnetic flux flows out. Between $t = 7.5$

and $t = 11.25$, the only source of the destruction of the net toroidal magnetic flux is magnetic reconnection due to the numerical diffusion. If we fit it as $\psi_t(t)/\psi_t(t=0) \equiv \exp(-t/\tau_{\rm res})$, the "resistive" dissipation time due to numerical diffusion is $\tau_{\rm res} \sim 10.9$. Therefore the numerical diffusion is not important on the time scales of CT transit time ($t \sim 5$) given injection speed $v_{\rm inj} = 1.1$. This implies that CT keeps almost intact before it arrives at its final position. The mixing between the CT and background plasma does not happen until the late compression stage.

IV. CONCLUSIONS & DISCUSSION

In this paper we presented nonlinear ideal MHD simulation results of a compact toroid injected into a hot strongly magnetized plasma. The simulations are intended to provide insights into CT fueling of an ITER-class tokamak. As a first step, we have investigated the problem of a high density low β CT injected into a slab background plasma with uniform magnetic field. We intend to investigate the injection of high β CT's as well as unmagnetized dense plasma jets, and also incorporate more realistic background profiles in follow-on work.

Our main findings are as follows. A regime is identified in terms of CT injection speed and CT-to-background magnetic field ratio that appears promising for precise core fueling. Shock-dominated regimes, which are probably unfavorable for tokamak fueling, are also identified. The CT penetration depth is proportional to the CT injection speed and density. For the regime identified as favorable for precise core fueling, the entire CT evolution can be divided into three stages: (1) initial penetration, (2) compression in the direction of propagation and reconnection, and (3) coming to rest and spreading in the direction perpendicular to injection. Tilting of the CT is not observed due to the fast transit time of the CT across the background plasma. Reconnection occurring at the upper left and lower right portions of the CT fragments the CT and leads to CT plasma outflow horizontally along the background magnetic field lines, forming a line-shaped structure almost parallel to the background magnetic field. We have also studied how the penetration depth is determined and have found an empirical relationship between the penetration depth versus the initial injection speed and CT plasma density. The penetration depth is proportional to the injection speed and CT density. When the CT comes to rest, it is highly compressed in the direction of injection, implying that very precise deposition is possible.

In a device with high bootstrap current fraction, optimized density and pressure profiles must be maintained. A core fueling system is all that a burning plasma may have to alter core plasma conditions and for burn control. Initial density peaking via core fueling provides more flexibility to reach ignition. If a CT injection system is within the ITER-relevant, no-shock/wavefront regime as required by $V_{\rm AC} < v_{\rm inj} \ll V_{\rm AP}$, $\rho_b/\rho_p \lesssim 15$ and $B_b/B_p \ll 1$, then precise core deposition with minimal background equilibrium perturbation may be possible.

Finally, let us evaluate our simulation results in the context of National Spherical Torus Experiment (NSTX) parameters. In this case, we assume that the CT plasma consists of 100% deuterium. Invoking NSTX parameters,[34] our dimensionless parameters would have the background plasma density $\rho_p = 0.1$ to be $1 \times 10^{14}\,{\rm cm}^{-3}$, tokamak field magnitude $B_p = 1.0$ to be $\sim 0.18\,{\rm T}$ and minor radius $a = 10$ to be $\sim 1\,{\rm m}$. Therefore, the CT radius $r_b = 1$ to be $10\,{\rm cm}$, number density $\rho_b = 1$ to be $1 \times 10^{15}\,{\rm cm}^{-3}$, CT field magnitude $B_b = 0.1$ to be $\sim 0.018\,{\rm T}$ and CT injection speed $v_{\rm inj} = 1.1$ to be $306\,{\rm km\,s}^{-1}$. The parameters are close to one proposed CT injection test on NSTX, which from Fig. 8(a) gives a penetration depth around 54 cm. A CT will do far more localized fueling on a NSTX-sized device. Note that previous experiments were too small to study localized core fueling. Given the ITER parameters (Table.I), $V_{\rm AC} \sim 1700\,{\rm km\,s}^{-1}$ is far higher than the accessible injection speed ~ 400 km s^{-1} from the current injector. Thus for CT fueling into a large, strongly magnetized tokamak like ITER, the ratio of ρ_b/ρ_p should be at least $\gtrsim 100$ to have a reasonably low $V_{\rm AC}$ for penetration to happen. This is by all means a big engineering chanllenge. From Fig. 8(b), a simulation with such a large ρ_b/ρ_p needs a larger computation domain and thus larger resolution. This will be considered in follow-on work.

Acknowledgments

The authors would like to thank Shengtai Li for the extensive advice on the code. The authors would also like to thank Roger Raman and Xianzhu Tang for their very inspiring discussion and constructive comments. This work was funded by DOE contract no. DE-AC52-06NA25396 under the Los Alamos Laboratory Directed Research and Development

(LDRD) Program.

---

[1] P. B. Parks, Phys. Rev. Lett. **61**, 1364 (1988).

[2] R. Raman and P. Gierszewski, Fusion Eng. Des. **39-40**, 977 (1998).

[3] S. L. Milora, C. A. Foster, P. H. Edmunds, and G. L. Schmidt, Phys. Rev. Lett. **42** (1979).

[4] L. J. Perkins, S. K. Ho, and J. H. Hammer, Nucl. Fusion **28**, 1365 (1988).

[5] W. A. Newcomb, Phys. Fluids B **3**, 1818 (1991).

[6] Y. Suzuki, T. Hayashi, and Y. Kishimoto, Physics of Plasmas **7**, 5033 (2000).

[7] Y. Suzuki, T.-H. Watanabe, T. Sato, and T. Hayashi, Nuclear Fusion **40**, 277 (2000).

[8] Y. Suzuki, T. Hayashi, and Y. Kishimoto, Nuclear Fusion **41**, 873 (2001).

[9] Y. Suzuki, T.-H. Watanabe, T. Sato, and T. Hayashi, Nuclear Fusion **41**, 769 (2001).

[10] M. R. Brown and P. M. Bellan, Phys. Rev. Lett. **64**, 2144 (1990).

[11] M. R. Brown and P. M. Bellan, Nucl. Fusion **32**, 1125 (1992).

[12] R. Raman, F. Martin, B. Quirion, M. St-Onge, J.-L. Lachmbre, D. Michaud, B. Sawatzky, J. Thomas, A. Hirose, D. Hwang, et al., Phys. Rev. Lett. **73**, 3101 (1994).

[13] R. Raman, F. Martin, E. Haddad, M. St-Onge, G. Abel, C. Côte, N. Richard, N. Blanchard, H. Mai, B. Quirion, et al., Nuclear Fusion **37**, 967 (1997), URL `http://stacks.iop.org/0029-5515/37/967`.

[14] R. Raman, F. Martin, G. Pacher, B. Stansfield, P. D. Michaud, Gierszewski, C. S. Pitcher, J. L. Lachambre, C. Côté, G. Abel, et al., in *in Controlled Fusion and Plasma Physics Proceedings of 24th Europe Conference, Berchtesgaden, 1997* (Europe Physical Society, Geneve, 1999), vol. 21A, Part I.

[15] M. J. Gouge, D. Q. Hwang, L. R. Baylor, S. K. Combs, P. W. Fisher, C. R. Foust, S. L. Milora, H. S. Mclean, R. D. Horton, R. W. Evans, et al., in *Proceedings of 16th International Conference, Montreal, 1996* (International Atomic Energy Agency, Vienna, 1997), vol. 3.

[16] N. Fukumoto, N. Fujiwara, K. Kuramoto, M. Ageishi, M. Nagata, T. Uyama, H. Ogawa, S. Kasai, K. Hasegawa, and T. Shibata, in *Bull. Amer. Phys. Soc.* (1997), vol. 42, p. 1961.

[17] J. T. Slough and A. L. Hoffman, in *Proceedings of 16th International Conference, Montreal, 1996* (International Atomic Energy Agency, Vienna, 1997), vol. 2.

[18] R. Décoste, Y. Demers, J.-L. Lachambre, G. Pacher, J. L. Gauvreau, A. Côté, C. Côté, G. Abel,

I. Condrea, C. Boucher, et al., in *Proceedings of 17th IAEA Fusion Energy Conference, Yokohama, 1998* (International Atomic Energy Agency, Vienna, 1998).

[19] D. Q. Hwang, M. Ryutova, and H. McLean, Phys. Plasmas **6**, 1515 (1999).

[20] T. Ogawa, N. Fukumoto, M. Nagata, H. Ogawa, M. Maeno, K. Hasegawa, T. Shibata, T. Uyama, J. Miyazawa, S. Kasai, et al., Nuclear Fusion **39**, 1911 (1999), URL `http://stacks.iop.org/0029-5515/39/1911`.

[21] D. Q. Hwang, H. S. McLean, K. L. Baker, R. W. Evans, R. D. Horton, S. D. Terry, S. Howard, and G. L. Schmidt, Nucl. Fusion **40**, 897 (2000).

[22] J. T. Slough and A. L. Hoffman, Phys. Plasmas **6**, 253 (1999).

[23] C. Xiao, A. Hirose, and S. Sen, Phys. Plasmas **11**, 4041 (2004).

[24] M. Nagata, H. Ogawa, S. Ystsu, N. Fukumoto, H. Kawashima, K. Tsuzuki, N. Nishino, T. Uyama, Y. Kashiwa, T. Shibta, et al., Nucl. Fusion **45**, 1056 (2005).

[25] D. Liu, C. Xiao, A. K. Singh, and A. Hirose, Nucl. Fusion **46**, 104 (2006).

[26] G. Olynyk and J. Morelli, Nuclear Fusion **48**, 095001 (2008).

[27] International Atomic Energy Agency, Tech. Rep., International Atomic Energy Agency (2001), No. 19 in the ITER EDA Documentation Series.

[28] M. Ono, M. Peng, C. Kessel, C. Neumeyer, J. Schmidt, J. Chrzanowski, D. Darrow, L. Grisham, P. Heitzenroeder, T. Jarboe, et al., Nuclear Fusion **44**, 452 (2004), URL `http://stacks.iop.org/0029-5515/44/452`.

[29] F. Wagner et al, in *Proceedings of the 13th Conference on Plasma Physics and Controlled Nuclear Fusion Research* (IAEA, Vienna, 1982), vol. 1.

[30] S. Li, H. Li, and R. Cen, ApJS **174**, 1 (2008).

[31] H. Li, G. Lapenta, J. M. Finn, S. Li, and S. A. Colgate, Astrophys. J. **643**, 92 (2006).

[32] P. M. Bellan, *Spheromaks* (Imperial College Press, London, 2000).

[33] W. Liu, S. C. Hsu, H. Li, S. Li, and A. G. Lynn, Phys. Plasmas **15**, 072905 (2008).

[34] R. Kaita, D. Johnson, L. Roquemore, M. Bitter, F. Levinton, F. Paoletti, and D. Stutman, IEEE TRANSACTIONS ON PLASMA SCIENCE **30**, 219 (2002).

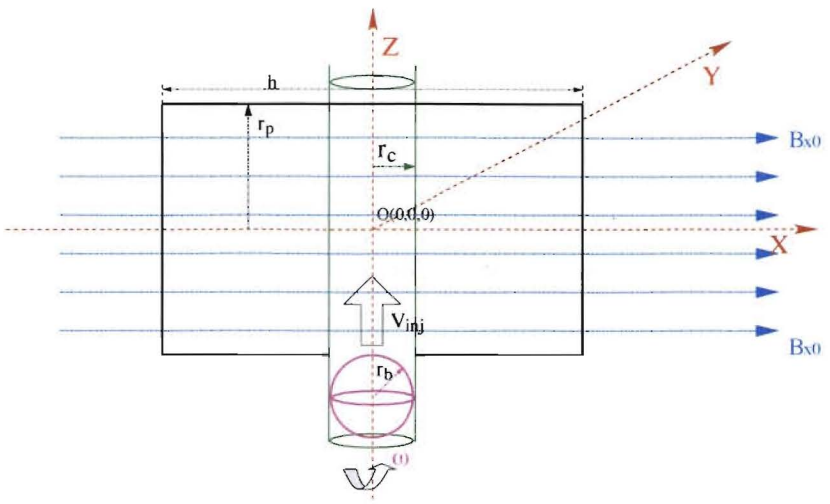

Figure 1: Schematic of the simulation geometry showing the coordinate system. In the texts, the direction along $z-$axis is defined as axial direction. $x-y$ plane is defined as the toroidal plane while $x-z$ plane is defined as the poloidal plane.

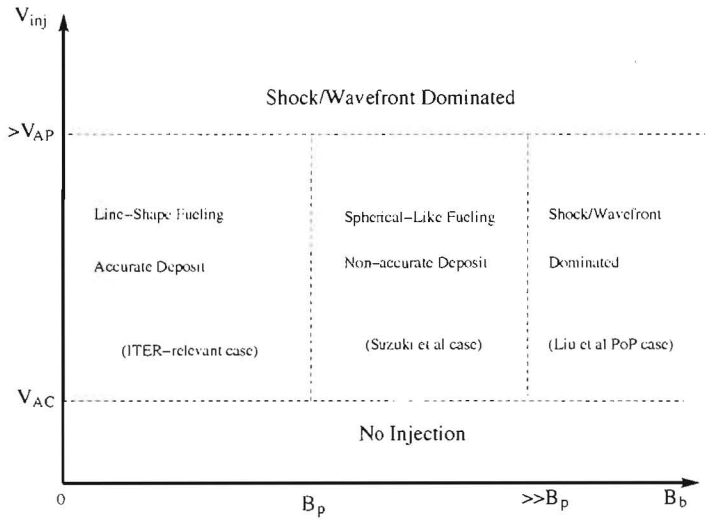

Figure 2: Qualitative behavior for CT injection in terms of CT injection speed and magnetic field strength.

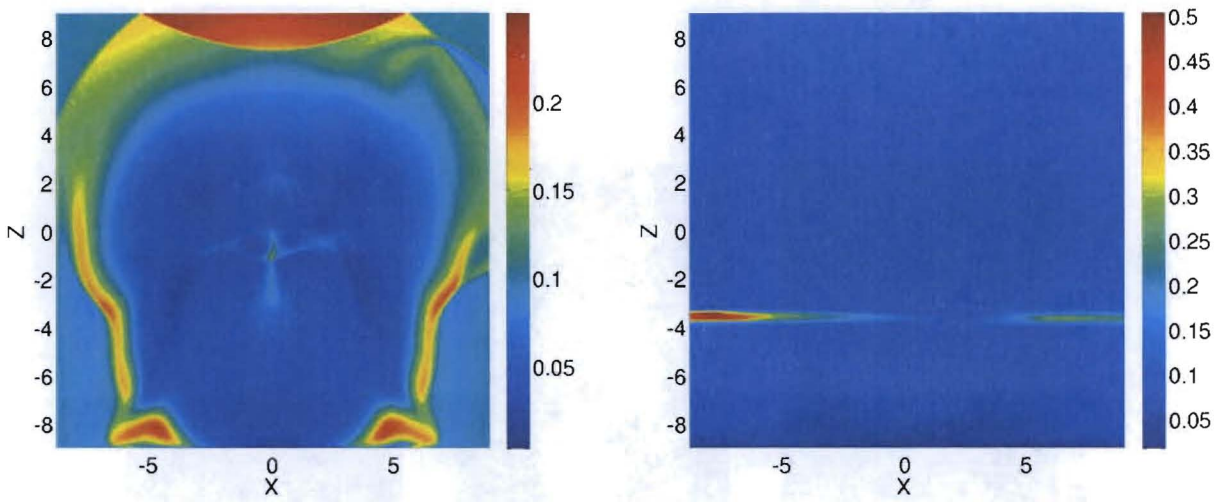

Figure 3: (color) Density (in common logarithmic scale) in the x-z plane. *Left* panel: at $t = 2.5$ with injection speed $v_{\rm inj} = 10.0$, which gives out non-localised deposition. *Right* panel: at $t = 20$ with injection speed $v_{\rm inj} = 1.1$, which gives out localized deposition. z is the injection direction.

Table I: Normalized Physical Quantities. Note that $V_{\rm AC} = B_p/\sqrt{\rho_b} = 1.0$. Injection speed $v_{\rm inj}$ is between $V_{\rm AC}$ and $V_{\rm AP}$.

	CT		Background	
Physical Quantities	numerical	physical	numerical	physical
Magnetic Field	$B_b = 0.1$	$B_b = 0.53$ T	$B_p = 1.0$	$B_p = 5.3$ T
Density	$\rho_b = 1.0$	$\rho_b = 1.86 \times 10^{15}$ cm^{-3}[a]	$\rho_p = 0.1$	$\rho_p = 1.86 \times 10^{14}$ cm^{-3}
Temperature	$T_b = 0.001$	$T_b = 75$ ev	$T_p = 0.1$	$T_p = 7.5$ kev
plasma $\beta = 2\rho T/ < B^2 >$	$\beta_b = 0.2$		$\beta_p = 0.02$	
Alfvén Speed $V_{\rm A} = B/\sqrt{\rho}$	$V_{\rm AB} = 0.1$	$V_{\rm AB} = 170$ km s^{-1}	$V_{\rm AP} = 3.16$	$V_{\rm AP} = 5.4 \times 10^3$ km s^{-1}
Sound Speed $V_c = \sqrt{\gamma T}$	$V_{\rm cB} = 1.7 \times 10^{-3}$	$V_{\rm cB} = 2.89$ km s^{-1}	$V_{\rm cP} = 0.41$	$V_{\rm cP} = 7.0 \times 10^2$ km s^{-1}

[a]plasma is assumed to be composed of half deuterium and tritium. The plasma density is the sum of electron and ion densities.

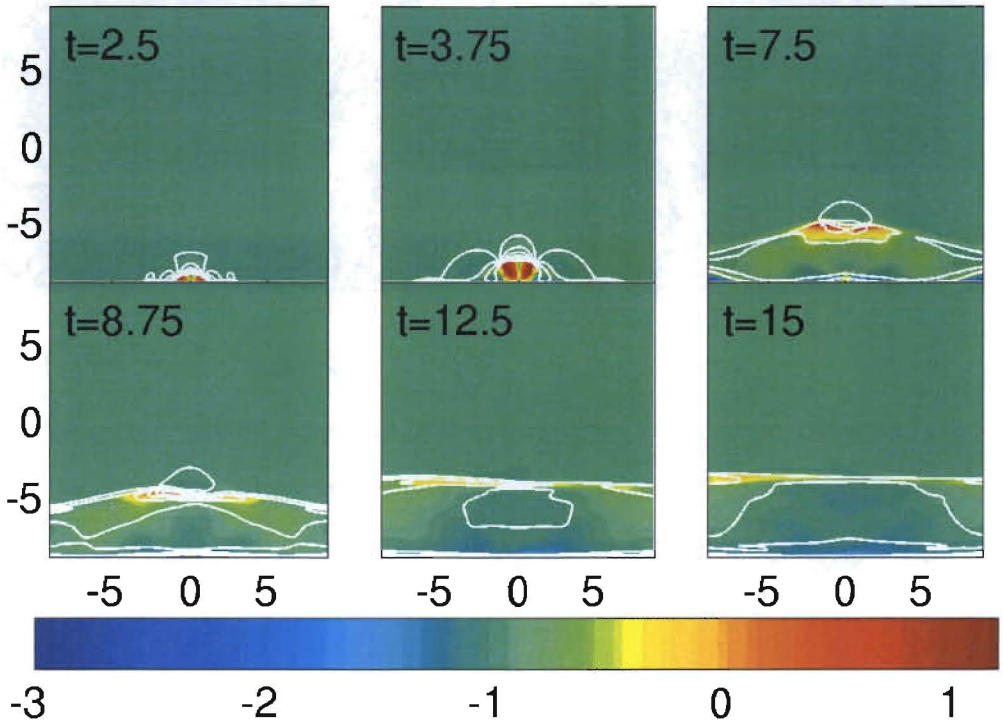

Figure 4: (color) Density (in common logarithmic scale) in the x-z plane with $y = 0$ as a function of time ($\alpha = \sqrt{10}$). The white solid contour lines indicate the magnetic pressure $p_B = B^2/2$. $t = 2.5$, $p_B \in [0.0, 1.6843]$; $t = 3.75$, $p_B \in [0.0, 1.7612]$; $t = 7.5$, $p_B \in [0.0, 1.4405]$; $t = 8.75$, $p_B \in [0.0, 1.1872]$; $t = 12.5$, $p_B \in [0.0, 1.0219]$; $t = 15$, $p_B \in [0.0, 1.008]$. The number of the contour levels are all 15.

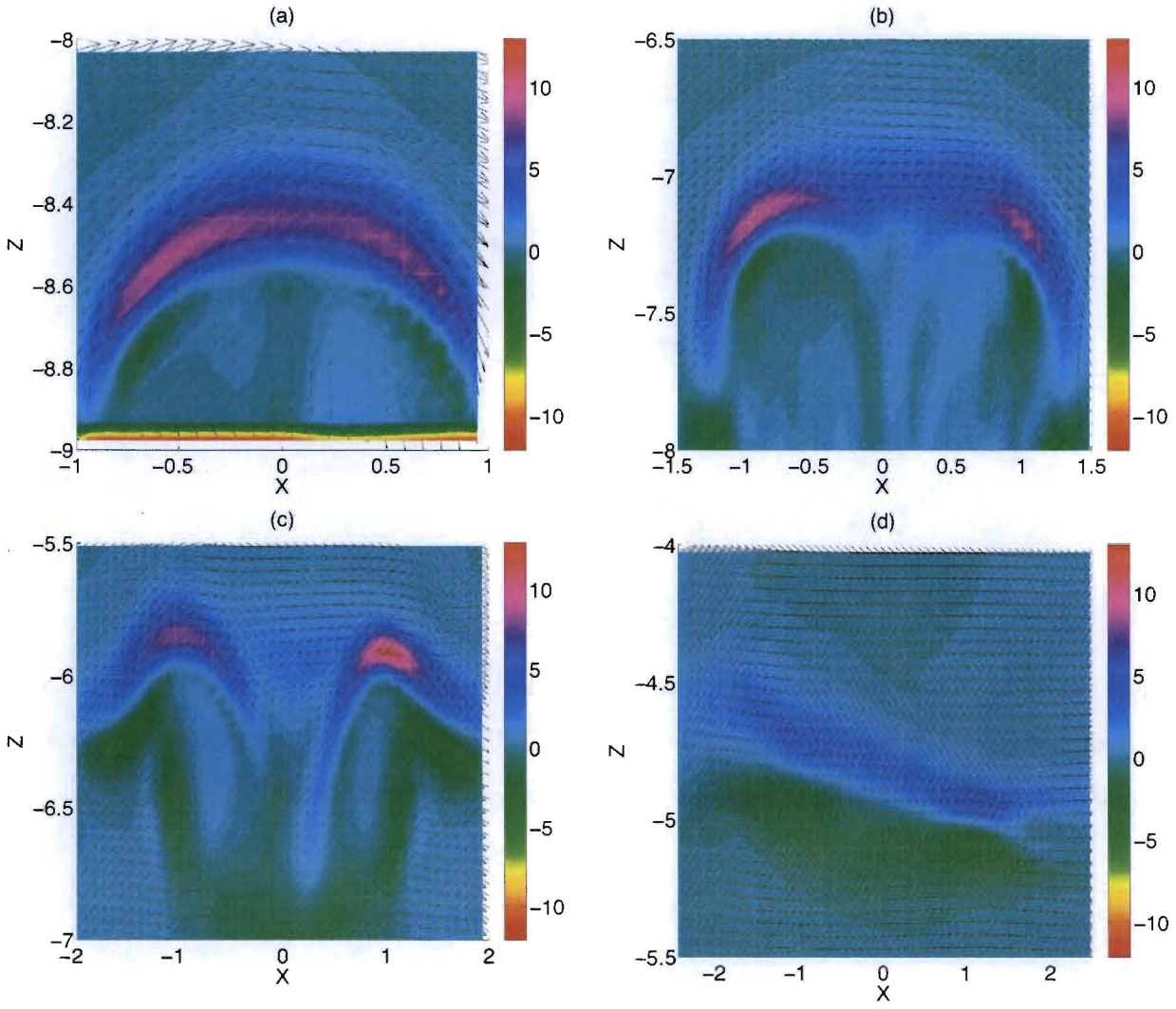

Figure 5: (color) Poloidal magnetic field and y-direction current density j_y in the x-z plane as a function of time ($\alpha = \sqrt{10}$). The color contours indicate j_y while arrows indicate B_x and B_z. B_x and B_z are normalized to their maximum values. (a) $t = 2.5$; (b) $t = 4.375$; (c) $t = 6.25$; (d) $t = 8.75$.

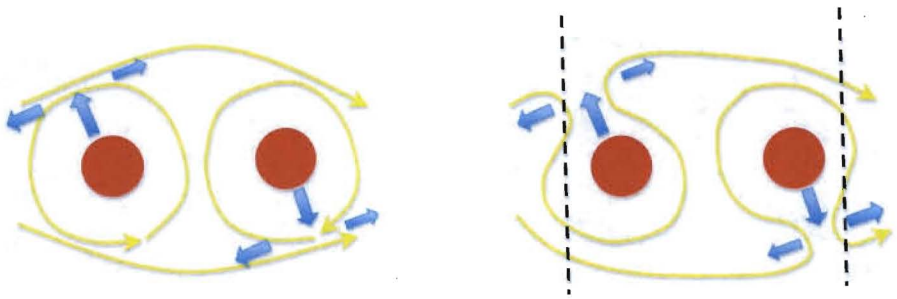

Figure 6: (color) Diagram of magnetic configuration in the contraction stage. Red color indicates the high-density CT plasma at shifted double peaks. Yellow lines indicate the magnetic field lines while blue arrows indicate the CT plasma flow patterns.

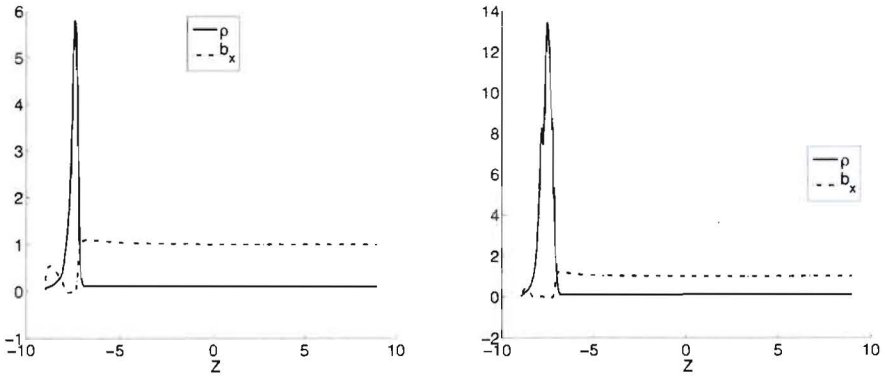

Figure 7: Axial profiles in the z-direction of several quantities at $t = 4.375$ with $(x, y) = (-1.125, 0)$ (*left*) and $(x, y) = (0.845, 0)$ (*right*) . The density ρ and the x direction magnetic field strength B_x are shown for inspecting the magnetic configuration shown in Fig. 6(*right*). These two axial cuts correspond to the two dash lines in Fig. 6(*right*).

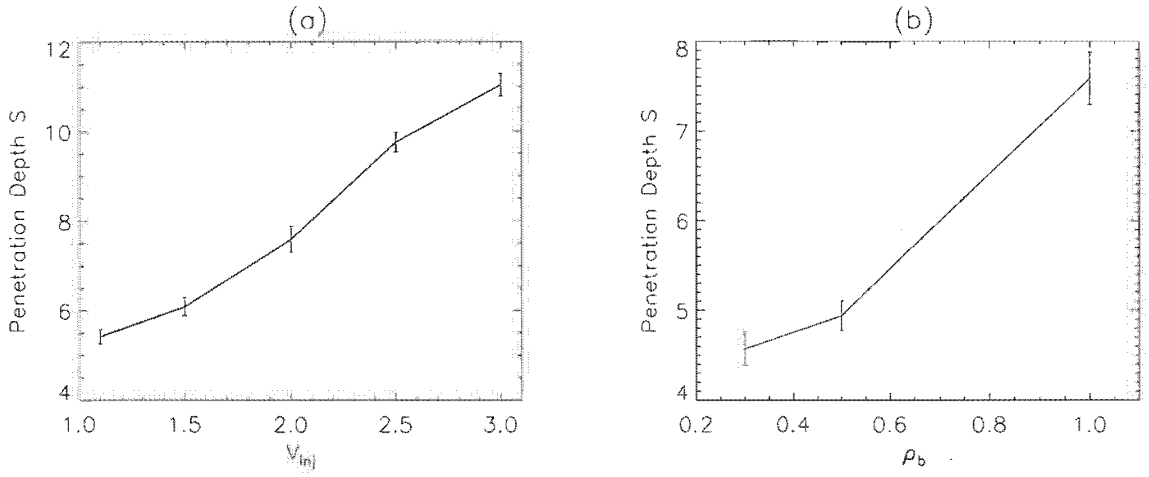

Figure 8: (a) Penetration Depth S *v.s.* Injection Speed $v_{\rm inj}$ with $\rho_b/\rho_p = 10$ and (b) Penetration Depth S *v.s.* CT Density ρ_b with $v_{\rm inj} = 2.0$. The penetration depth is defined as the distance between the final mean position of the injected plasma and the bottom boundary. The error bar indicates the spread of the line composed by the injection CT plasma.

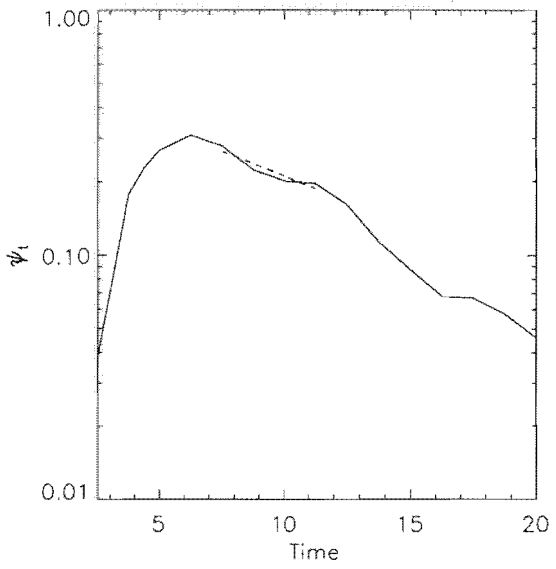

Figure 9: Decay of the net toroidal magnetic flux $\psi_t = \int B_y dS$, where only positive B_y is selected with $v_{\rm inj} = 1.1$ and $\rho_b/\rho_p = 10$. The dash line fits the data between $t = 7.5$ and $t = 11.25$ with the formula $\psi_t(t)/\psi_t(t=0) \equiv \exp(-t/\tau_{\rm res})$, where $\tau_{\rm res} = 10.9$ is the resistive dissipation time due to the numerical diffusion, and it is much larger than the CT transit time ~ 5 given injection speed $v_{\rm inj} = 1.1$. This implies that CT keeps almost intact before it arrives at its final position.